
When Perspective Comes for Free: Improving Depth Prediction with Camera Pose Encoding

Yunhan Zhao¹ Shu Kong² Charless Fowlkes¹

¹UC Irvine ²Carnegie Mellon University

{yunhaz5, fowlkes}@ics.uci.edu shuk@andrew.cmu.edu

[\[Project Page\]](#) [\[Github\]](#) [\[Slides\]](#)

Abstract

Monocular depth prediction is a highly underdetermined problem and recent progress has relied on high-capacity CNNs to effectively learn scene statistics that disambiguate estimation. However, we observe that such models are strongly biased by the distribution of camera poses seen during training and fail to generalize to novel viewpoints, even when the scene geometry distribution remains fixed. To address this challenge, we propose a factored approach that estimates pose first, followed by a conditional depth estimation model that takes an encoding of the camera pose prior (*CPP*) as input. In many applications, a strong test-time pose prior *comes for free*, e.g., from inertial sensors or static camera deployment. A factored approach also allows for adapting pose prior estimation to new test domains using only pose supervision, without the need for collecting expensive ground-truth depth required for end-to-end training. We evaluate our pose-conditional depth predictor (trained on synthetic indoor scenes) on a real-world test set. Our factored approach, which only requires camera pose supervision for training, outperforms recent state-of-the-art methods trained with full scene depth supervision on 10x more data.

1 Introduction

Predicting 3D scene geometry from a single image is a challenging perceptual task with broad applications in areas such as AR/VR [19, 17] and autonomous driving [27, 29]. Despite monocular depth prediction being a hugely underdetermined problem, supervised training of Convolutional Neural Nets (CNNs) have proven surprisingly effective [6, 5, 8, 11, 16, 28]. Training on sufficiently large-scale datasets (e.g., [22, 1, 3, 9]) allows predictive models to implicitly capture the joint statistics of scene geometry and appearance.

Despite remarkable progress, it is unclear when such models will robustly generalize to novel viewpoints and environments. Depth maps are a *view-dependent* representation of 3D scene geometry that depends strongly on both the statistics of scene geometry and the camera pose. Recent work in analyzing the visual cues used by learned depth prediction models [4] highlights that such models are highly sensitive to camera poses. We confirm this in our experiments (Sect. 4) where we show that depth predictors perform poorly when the training and testing sets have different camera pose distributions (despite the scene content remaining fixed).

Motivated by this observation, we propose to disentangle viewpoint and geometry by training two separate models, one that estimates a prior over camera pose and the other that estimates depth conditioned on pose (illustrated in Fig. 1). We encode the camera pose prior (**CPP**) as a *scene-independent* depth map which is passed as an additional input channel to the pose-conditioned depth estimator (Fig. 2). This factorized approach makes it possible to quickly adapt the depth predictor to test domains with significantly different camera pose statistics without retraining the model.

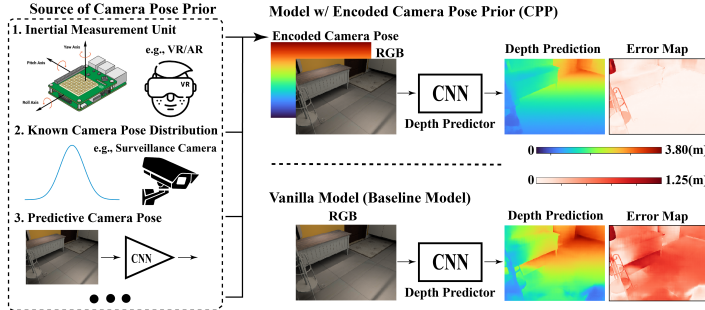


Figure 1: We propose to exploit camera pose as prior conditioned on which we train the depth predictor. The camera pose can be from sensors or estimated by camera pose predictors. We encode the camera pose as a 2D map that is *concatenated* with the image as input to a pose-conditional depth predictor. As seen in the prediction error map, by leveraging the pose prior CPP allows much better depth estimates compared to a vanilla baseline model that takes only RGB image as input. Figure 2 illustrates how the encoded map is computed from the camera pose priors.

While such a factorized model (i.e., CPP) is unlikely to yield better predictions than an end-to-end approach when training data is plentiful and well matched to the test distribution, we argue that a modular approach can yield better performance in many practical settings. First, it becomes straightforward to leverage additional side-information available at test-time. For many real-world applications, the test-time camera pose prior is quite constrained. Cameras mounted in fixed installations or on an autonomous vehicle platforms typically have a nearly constant tilt, roll and height above the ground plane. Inertial sensors and odometry provide quite accurate pose estimates for mobile or AR devices. Second, even when test-time pose doesn’t “come for free” in a new test domain, learning a camera pose prior for a new domain is likely to be “easier” than training an end-to-end depth model. While acquiring dense depth data for the new domain is expensive, ground-truth camera pose is low-dimensional and can be estimated without specialized sensors (e.g., via visual odometry).

We carry out extensive experiments on a synthetic indoor scene dataset (InteriorNet [18]) to demonstrate that leveraging camera pose can significantly improve training and prediction. Our factored model generalizes much better than a vanilla counterpart (i.e., a typical depth predictor w/o using camera poses) to a test set which has a different camera pose distribution from the training set. When a strong camera pose prior is not available during inference, utilizing a trained camera pose prediction model in combination with the conditional model yields predictions which are as good or better than the vanilla model. Finally, we evaluate our CPP model on a real-world test set sampled from ScanNet [3] with uniform camera poses. In this setting, the pose-conditional model trained solely on *synthetic data*, outperforms a recent state-of-the-art method [28], which is trained on *10x more real data*! This suggests that shifts in camera pose statistics may be more important than scene geometry or appearance in synthetic-to-real domain adaption.

2 Related Work

Monocular Depth Prediction has advanced significantly since the seminal works presented in [14, 24, 25]. Currently, one of the most effective approaches is to train a deep Convolutional Neural Net (CNN) over large-scale training data to predict monocular depth [6, 16, 8, 28]. There are multiple lines of work to improve monocular depth prediction. For example, [21] adopts coarse-to-fine architecture, [6] proposes multi-scale learning for better depth prediction, [8, 28] design sophisticated losses, [20, 17] collect larger-scale data, and [30, 32] leverage synthetic data. Surprisingly, *to the best of our knowledge, there isn’t work utilizing camera pose for monocular depth prediction*. This is perhaps due to the goal of learning a generic monocular depth predictor that works on any images. However, we note the camera pose information is ubiquitous, not only in public benchmarks like NYUv2 [22] and ScanNet [3], but also in real-world deployment scenarios, like AR/VR headsets and robotic platform-mounted cameras. Our work is motivated in part by exploring ways to take advantage of this freely available side-information during training (and testing).

Camera Parameter estimation plays an essential role in geometric computer vision tasks and has been used in a variety of learning-based approaches e.g., estimating camera pose for re-projection in self-supervised depth learning [10, 34] and jointly predicting camera motions and depth maps [26]. [13] address the effect of focal length differences in depth prediction by embedding focal length information into CNNs. [7] encode camera *intrinsic* parameters as an explicit input along with RGB, to learn a CNN depth predictor that adapts to different cameras. In contrast, we study the role of *extrinsic* camera parameters in monocular depth prediction and show that doing so enables our factorized CPP model to generalize much better to diverse test-time camera poses.

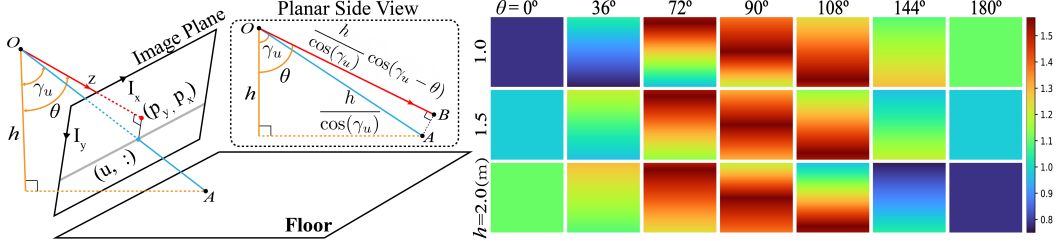


Figure 2: **Left:** We illustrate the proposed CPP which encodes camera pose (h, θ) as a 2D map with the same spatial resolution as the input image (Figure 1). The CPP encoding assumes the camera sits in an empty room which has an infinite floor and ceiling height as 3 meters. To compute this 2D encoding, we calculate the depth for each pixel (l_{OB} in the planar side view) as the distance (l_{OA}) projected onto onto the camera view axis z . See details in Section 3.2. **Right:** To visualize how the encoded maps change with different h and θ , we show encodings for a range of heights h (in meters) and pitches θ (in degrees).

3 Factored Depth Prediction

We propose a factorized approach that disentangles viewpoint statistics from depth predictions. Specifically, we encode camera pose priors (CPP) as *scene-independent* spatial maps that are later concatenated with RGB images as input to pose-conditional depth predictors.

3.1 Pose-Conditional Depth Prediction

Depth Prediction without Camera Poses (Vanilla Model) Typical CNN-based monocular depth models take a single RGB image x as input and outputs a depth map y with depth estimate at each pixel location. We denote the training set by $\mathcal{T} = \{x_i, y_i, \rho_i\}_{i=1}^N$, where x_i, y_i and ρ_i are the i^{th} RGB image, ground-truth depth map and camera pose respectively. We learn a vanilla model parameterized by σ_0 through maximum likelihood estimation:

$$\sigma_0^* = \arg \max_{\sigma_0} \mathbb{E}_{(x,y) \sim \mathcal{T}} [p(y|x; \sigma_0)]. \quad (1)$$

Under the assumption that $p(y|x; \sigma_0)$ follows, e.g. a Laplace distribution, the prediction model is fit by minimizing L_1 loss $l(\sigma_0) = \|f_{\sigma_0}(x) - y\|_1$ where $f_{\sigma_0}(\cdot)$ is the depth predictor instantiated as a CNN.

Depth Predictors Conditioned on Camera Pose Prior (CPP) When the camera pose ρ is available, we can fit a pose-conditional depth predictor parameterized by σ :

$$\sigma^* = \arg \max_{\sigma} \mathbb{E}_{(x,y,\rho) \sim \mathcal{T}} p(y|x, \rho; \sigma) \quad (2)$$

Without loss of generality, given some camera pose prior $p(\rho)$ at test time, we can take as our estimate the most probable depth for test sample x_j as:

$$y_j^* = \arg \max_{y' \in \mathcal{Y}} \int p(y'|x_j, \rho; \sigma^*) p(\rho) d\rho, \quad (3)$$

When the pose ρ^* is known at test time (e.g., fixed camera position), we have $p(\rho) = \delta(\rho - \rho^*)$ and $y_j^* = \arg \max_{y' \in \mathcal{Y}} p(y'|x_j, \rho^*; \sigma^*)$

Depth Predictors Conditioned on Predictive Camera Pose Prior (CPP_{pred}) When pose is available during training but not during test, we propose to train a separate camera pose predictor for the testing domain parameterized by τ :

$$\tau^* = \arg \max_{\tau} \mathbb{E}_{(x,\rho) \sim \mathcal{T}} [p(\rho|x; \tau)] \quad (4)$$

Swapping in the predicted camera pose prior, we predict monocular depth y_j^* for a test sample x_j as below:

$$y_j^* = \arg \max_{y' \in \mathcal{Y}} \int p(y'|x_j, \rho; \sigma^*) p(\rho|x_j; \tau^*) d\rho. \quad (5)$$

In our experiments, we also model $p(\rho|x_j; \tau)$ with a CNN and simply evaluate the conditional model at the point estimate $\rho^* = \arg \max_{\rho} p(\rho|x; \tau^*)$.

3.2 Representing and Encoding Camera Pose Priors

Camera pose is described by the translation and rotation of the camera with respect to some arbitrary global coordinate system (6-DoF). For typical terrestrial man-made scenes (indoors or outdoor urban scenes), we can take one coordinate axis to be upwards (as specified by gravitational acceleration) and fix the origin along that axis to be 0 at the ground-plane. Since there is no unique origin along the two remaining axes, we assume that our camera pose prior $p(\rho)$ should be uniform over translations parallel to the ground-plane. Similarly, there is no unique way to specify the orientation of the axes about the up-axis. This leaves on three degrees-of-freedom: the height of the camera above the ground-plane h , the pitch (angle relative to the up-axis) of the camera θ , and any roll ω of the camera around its optical axis.¹

Naive pose encoding Our conditional depth predictor makes use of camera pose as priors. However, it is non-trivial to use the camera pose vector as input to the depth predictor, which is typically a "fully" convolutional network. Inspired by the literature that converts sparse signals into a spatial map to better exploit the convolution-based computation [7, 29], we propose to encode the camera pose into $H \times W$ maps of the same spatial resolution as the input RGB image.

A naive encoding method is to simply copy the value of θ and h into separate channels of $H \times W$, i.e., we derive two maps encoding the camera height and pitch by $\mathbf{M}_\theta[:, :] = \theta$ and $\mathbf{M}_h[:, :] = h$, respectively. However, the effect of pose on the depth distribution depends strongly on the position in the image relative to the camera center so translation-equivariant convolutions cannot fully exploit this encoding (except by relying on boundary artifacts). This is supported by an experimental comparison (supplemental material) showing this naive encoding is inferior to our proposed *CPP* encoding method, elaborated in the following.

CPP encoding encodes pose locally by assuming that the camera is placed in an empty indoor scene with an infinite floor and ceiling² and uses the depth map of this generic scene as the encoding of pose. This provides a "default" depth estimate based on the camera pose which can be further refined locally by the conditional model based on image appearance. We illustrate the computation of this encoding in Figure 2. Concretely, knowing the principle point (p_y, p_x) and focal length f of the camera, we compute the angle between the gravity direction and the ray at the u^{th} row in the image plane (assuming no camera roll) as:

$$\gamma_u = \theta - \tan^{-1}\left(\frac{u - p_y}{f}\right), \quad \forall u \in [0, H] \tag{6}$$

We compute depth values at the u^{th} row in the encoded map $\mathbf{M} \in \mathbb{R}^{H \times W}$ as:

$$\mathbf{M}[u, :] = \begin{cases} \frac{h}{\cos(\gamma_u)} \cos(\gamma_u - \theta) & \gamma_u < \frac{\pi}{2} \\ +\infty & \gamma_u = \frac{\pi}{2} \\ \frac{C-h}{\cos(\pi - \gamma_u)} \cos(\gamma_u - \theta) & \gamma_u > \frac{\pi}{2} \end{cases} \tag{7}$$

where the term $\cos(\gamma_u - \theta)$ projects the distance to camera center onto camera view direction z to get depth values and C is the height of the ceiling. The depth map \mathbf{M} has values that converge to infinite depth at the horizon (i.e., when $\gamma_u \rightarrow \frac{\pi}{2}$). To map values into a finite range, we apply the inverse tangent operator $\tan^{-1}(\cdot)$ to obtain our final encoding $\mathbf{M}_{CPP} = \tan^{-1}(\mathbf{M})$ which takes on values in the range $[\tan^{-1}(\min\{h, C - h\}), \frac{\pi}{2}]$.

4 Experiments

To analyze the effect of camera pose on depth estimation, we carried out a systematic analysis using a dataset of synthetic indoor scenes with diverse camera poses. We then show that our factored model can achieve superior generalization to new real-world scene distributions with significantly less training data.

¹In the datasets we analyzed, camera roll was constant or showed very small variation so we ignore it in the subsequent paper. However, our encoding approach generalizes in a trivial manner to also encode roll (i.e., by simply rotating the encoded image around the principal point).

²For outdoor scenes one would eliminate the ceiling

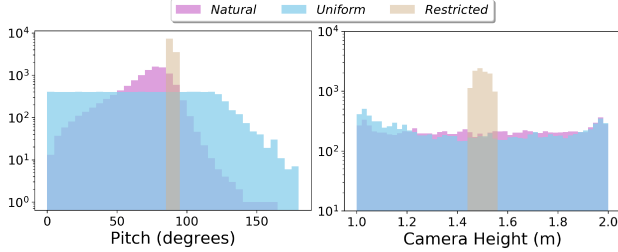


Figure 3: Distribution of camera pitch and heights for three subsets of images from InteriorNet. We adopt a stratified sampling technique to avoid picking adjacent video frames, and sample images from separate scenes for the 10k train and 1k test sets. *Natural* sample images at random, following the default InteriorNet distribution; *Uniform* samples images uniformly w.r.t. camera pitch; *Restricted* uses only samples images within a narrow range, i.e., pitch $\theta \in [85^\circ, 95^\circ]$ and height $h \in [1.45, 1.55]$ (meters).

Implementation. We adopt the UNet structure [35] and ResNet18 [12] as the network architectures for our depth predictor and pose predictor respectively. We resize all images and depth maps to 240×320 , and adjust camera intrinsic parameters (for CPP encoding) accordingly. We train all models for 200 epochs, using the Adam optimizer [15] with initial learning rate $1e-3$, and coefficients 0.5 and 0.999 for computing running averages of gradient and its square. We augment training data with random left-right flipping. We set the ceiling height $C = 3$ meters to compute the CPP encoding. Models are implemented in PyTorch [23] and trained on a single Titan X GPU.

Evaluation Metrics. For evaluation, we report several established metrics [6], including absolute relative difference (Abs-Rel), squared relative difference (Sq-Rel), root mean squared log error (RMS-log), and accuracy with a relative error threshold of $\delta^k < 1.25^k, i = 1, 2$. We list the detailed formula of computing these metrics in below with T representing the collection of test-time pixels to evaluate in ground-truth depth maps. Experimental results with additional evaluation metrics are shown in the supplementary material.

$$\begin{aligned} \text{Abs-Rel: } & \frac{1}{|T|} \sum_{y \in T} |y - y^*| / y^* & \text{Sq-Rel: } & \frac{1}{|T|} \sum_{y \in T} \|y - y^*\|^2 / y^* \\ \text{RMS-log: } & \sqrt{\frac{1}{|T|} \sum_{y \in T} \|\log y - \log y^*\|^2} & \delta^k: & \text{Fraction of } y \text{ s.t. } \max\left(\frac{y_i}{y_i^*}, \frac{y_i^*}{y_i}\right) < 1.25^k \end{aligned}$$

4.1 Datasets

InteriorNet [18] is a large-scale indoor scene dataset of photo-realistic synthetic video sequences with randomly generated camera trajectories. To analyze the effect of camera pose distribution, we sample three subsets of images from the complete InteriorNet dataset according to pre-defined distributions, as visualized in Figure 3. For each subset, we sample training (10k images) and testing images (1k images) from disjoint scenes and use a stratified sampling approach to avoid picking adjacent video sequence frames.

- *Natural* contains images whose camera poses follow the natural distribution of InteriorNet.
- *Uniform* samples images w.r.t camera pitch following uniform distribution. We divide the range of pitch into 36 bins, and sample an equal number of images from each. This yields a nearly uniform distribution except for some extreme pitch angles which were underrepresented in the original data.
- *Restricted* samples images which fall in a narrow range of camera pitch $\theta \in [85^\circ, 95^\circ]$ and height $h \in [1.45, 1.55]$ (meters).

ScanNet [3] is a real-world RGB-D video dataset contains millions of views in 1,513 indoor scenes with recorded true camera poses per frame. We randomly sample a test-set of 1k images according to a *uniform* distribution w.r.t camera pitch. We use this as a held-out dataset to validate the performance of the synthetically trained CPP model and compare to existing state-of-the-art depth predictors, including models trained on the NYUv2 [22] dataset. InteriorNet, NYUv2, and ScanNet all contain indoor scene images with camera models that have similar intrinsics. For a detailed comparison of these three datasets, please refer to the supplementary material.

4.2 Analyzing Influence of Pose Distributions and Priors

CPP Improves Depth Predictions. Table 1 shows depth prediction performance of the vanilla model, CPP which encodes the true camera pose, and CPP_{pred} which encodes the predicted pose. We summarize primary observations

- By encoding camera pose prior, CPP significantly outperforms the vanilla baseline model when both are trained and tested on the same pose distribution (e.g., compare CPP-N and Vanilla-N evaluated on *Natural* test-set). The left pane of Figure 4 shows qualitative examples where CPP greatly improves on the depth predictions of the vanilla baseline.

Models	Natural test-set (N)		Uniform test-set (U)		Restricted test-set (R)	
	↓ better Abs-Rel/Sq-Rel/RMS-log	↑ better δ^1 / δ^2	↓ better Abs-Rel/Sq-Rel/RMS-log	↑ better δ^1 / δ^2	↓ better Abs-Rel/Sq-Rel/RMS-log	↑ better δ^1 / δ^2
Vanilla model – no camera pose encoding						
Vanilla-N	.154 / .148 / .229	.803 / .945	.183 / .146 / .250	.724 / .926	.155 / .233 / .284	.804 / .916
Vanilla-U	.169 / .173 / .250	.767 / .935	.161 / .117 / .227	.758 / .950	.178 / .283 / .325	.764 / .898
Vanilla-R	.259 / .349 / .392	.551 / .786	.284 / .307 / .376	.506 / .779	.147 / .230 / .286	.820 / .918
Encoding model – camera pose prior (CPP)						
CPP-N	.108 / .120 / .199	.872 / .958	.106 / .088 / .183	.876 / .961	.155 / .244 / .285	.806 / .918
CPP-U	.129 / .150 / .221	.842 / .945	.102 / .087 / .177	.889 / .966	.178 / .303 / .322	.773 / .901
CPP-R	.223 / .263 / .308	.651 / .879	.249 / .275 / .312	.620 / .873	.142 / .213 / .274	.828 / .919
Encoding model – predicted camera pose prior (CPP _{pred})						
CPP _{pred} -N	.146 / .134 / .218	.820 / .954	.166 / .121 / .231	.762 / .944	.156 / .234 / .286	.803 / .918
CPP _{pred} -U	.168 / .187 / .252	.779 / .934	.148 / .115 / .213	.806 / .953	.196 / .338 / .333	.747 / .891
CPP _{pred} -R	.266 / .350 / .389	.554 / .789	.308 / .347 / .394	.486 / .754	.143 / .214 / .276	.827 / .918

Table 1: **Systematic analysis of the effect of training set pose distribution on prediction.** We train and test models on different datasets that have different camera pose distributions (i.e., our sampled three subsets). We report the performance of vanilla baseline model, CPP and CPP_{pred}. CPP-N/U/R represents the CPP model trained with *Natural/Uniform/Restricted* train-set. We observe that models trained on restricted pose data generalize poorly, conditioning on known camera pose significantly improves performance, and conditioning on predicted pose performs as well or better than the end-to-end trained baseline model.

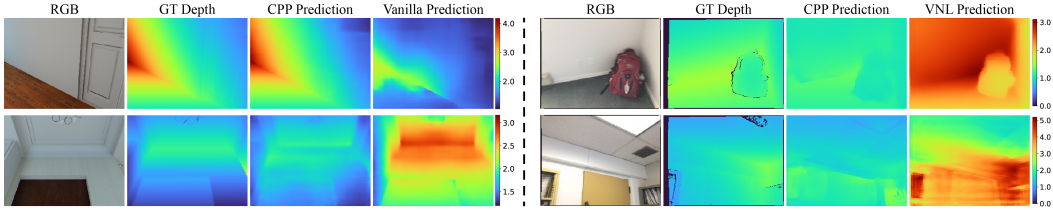


Figure 4: Visualization of depth prediction results on InteriorNet (left) and ScanNet (right). We compare our CPP predictions against the vanilla baseline model and VNL (a recently released state-of-the-art model trained on 120k real-world RGBD images [28]). Despite being only trained on smaller quantities of synthetic data, CPP provides much better predictions, particularly in cases shown here with more extreme camera viewpoints.

- Comparing CPP-R and Vanilla-R evaluated on *Restricted* test-set, CPP only shows subtle performance gain over the vanilla model (compared to the boost seen on *Natural* and *Uniform* subsets). When the pose distribution is already tightly constrained, the pose prior doesn’t provide additional information.

CPP Improves Generalization to Novel Camera Poses. CPP uses a factorized model that effectively addresses the issue of camera pose distribution changes by swapping in new, appropriate camera pose priors at test time. To summarize salient cross-dataset results from Table 1:

- CPP models show improved generalization ability as they outperform vanilla models without explicitly training on the same camera pose distribution in the evaluation sets. For example, compare the performance of CPP-N and Vanilla-U evaluated on *Uniform* test-set. CPP-N is trained on *Natural* train-set, but outperforms Vanilla-U when evaluated on the *Uniform* test-set! Similarly, CPP-U outperforms Vanilla-N evaluated on *Natural* test-set. These observations illustrate that CPP models generalize well to other camera pose distributions without the need for expensive retraining.
- When trained on *Restricted* train-set, CPP-R is no longer able to outperform the Vanilla-N/U models evaluated on on *Natural* or *Uniform* test-sets. This is presumably because CPP-R overfits to the camera poses presented in *Restricted* train-set.
- Models trained on *Restricted* show substantially worse performance on new test-sets with diverse camera poses (*Uniform* or *Natural*). The performance gap between diverse and restricted models is much smaller on *Restricted* test data (e.g., the relative gap in Abs-Rel between the best and worse model is 5-10x smaller on test set R). This asymmetry suggests exposure to diverse camera pose conditions during training are crucial to learning better depth predictors.

Encoding with Predicted Camera Poses. When true camera pose is unknown at test time, we substitute an independent image-based camera-pose predictor trained on the camera pose distribution of interest. As shown in Table 1, encoding such predictive pose prior allows CPP_{pred}-N/U to outperform the vanilla model on both within and cross-distribution tests performance. This suggests that the factored model can still maintain the same level of performance as the end-to-end trained vanilla baseline while offering more flexibility and generalization ability when stronger pose priors are available.

Resilience to Noise in Camera Pose. Erroneous camera pose prediction makes the performance of CPP_{pred} inferior to CPP with true camera pose. To further analyze the resilience of CPP to incorrectly specified pose, we examine the prediction performance when adding a random level of noise to the true camera pose using CPP-N. For each test image, we perturb the true camera pitch θ_{gt} and height

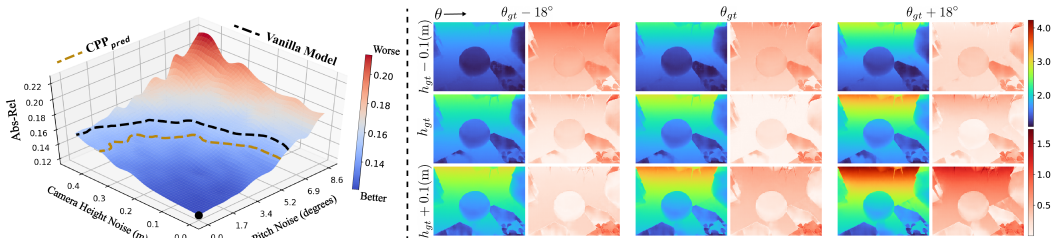


Figure 5: **Left:** We plot depth prediction performance (*Abs-Rel*) for different levels of camera height and pitch noise. For a given noise level ϵ , we compute predictions using pose encodings where, e.g. the pitch is sampled from $\theta_{gt} + \mathcal{U}[-\epsilon, \epsilon]$. The black dot at the origin shows the (best) performance with the true camera pose (i.e., no noise are presented in pitch and height). The dashed lines represent the average performance levels for the vanilla and CPP_{pred} models. **Right:** We visualize depth prediction by CPP with perturbed camera pitch angles $\theta_{gt} \pm 18^\circ$ and heights $h_{gt} \pm 0.1$ (m). CPP model predicts shallower depth when both pitch and camera height decrease (camera is tilted down or translated closer to the floor). This qualitatively confirms that the camera pose prior induces a meaningful shift in the estimator. The corresponding RGB image and ground-truth depth appear in Fig. 6.

Models	↓ better	↑ better
	Abs-Rel/Sq-Rel/RMS-log	δ^1 / δ^2
Avg	.414 / .641 / .466	.346 / .638
Blind	.342 / .519 / .395	.485 / .750
Img-1	.041 / .010 / .082	.946 / .999
Img-2	.115 / .059 / .176	.793 / .990

Table 2: Comparison between using the mean depth map computed on the *Natural* train-set and the “blind predictor”, which estimates depth solely from per-image encoded maps *without* RGB images. We report results on *Natural* test-set. We find that “blind predictor” performs better than “mean depth map”, implying the benefit of exploiting camera poses. We also report on two specific images on which “blind predictor” performs well, as shown in Figure 6. This further confirms the using camera poses is helpful when cameras are looking down on the floor and images have little texture cues for depth inference.

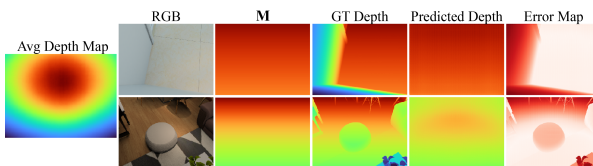


Figure 6: Visualizations of mean depth map of the *Natural* train-set, and two specific images with their encoded maps \mathbf{M} . By “blind prediction”, we train depth predictor solely over the encoded maps *without* input RGB images. Note that \mathbf{M} , gt depth maps, predicted depth maps and error maps are normalized to the same scale in each row for better visual comparison. By comparing \mathbf{M} and true depth maps, we can see \mathbf{M} presents nearly the true depth in floor areas. In other words, \mathbf{M} contains highly accurate depth information of floor/ceiling regions in the scene, providing a reliable prior information that helps depth prediction.

h_{gt} with uniform random noise ϵ whose magnitude ranges within ± 8.6 degrees in pitch and ± 0.4 in height. Figure 5 shows depth prediction performance as a function of the accuracy in camera pitch and height estimation. We find that CPP outperforms the vanilla model even with significant misspecification of the pose (e.g., height error < 0.3 m, pitch error < 5 degrees).

We also visualize example depth predictions produced by manually adding/subtracting an amount from true camera pitch and height in Figure 5. When the camera height and pitch decrease, the depth predictor tends to predict closer depth. This aligns with our intuition that, when the camera is looking down or moving towards the floor, the scene should be closer to the camera.

Predicting Depth from Pose Alone. To characterize how much information is contained in the camera pose alone, we train a “blind predictor” on the *Natural* which is provided with only the encoded pose but *without* any RGB input. For comparison, we also compute the mean depth map over the same *Natural* train-set. A quantitative evaluation is in Table 2. We also report prediction error on two specific images which are visualized in Figure 6. For camera poses such as these which contain relatively few objects or perspective cues (e.g., much floor or ceiling visible), the blind prediction can be quite accurate. Overall we see that camera pose reduces the absolute relative error by $\sim 20\%$ compared to simply predicting a constant (the mean).

4.3 Real-World Evaluation on ScanNet

We evaluate on the real-world test-set sampled from ScanNet, and compare against a recently published state-of-the-art method called VNL [28] which adopts a sophisticated loss function that enforces the “virtual surface normal” constraints during training. For a thorough comparison, we evaluate both the publicly-released VNL model trained on 120k real RGBD images of NYUv2 dataset [22] as well as retraining the VNL model on our InteriorNet train-sets.

ScanNet offers a strong test of generalization performance since none of the depth prediction models (Vanilla, CPP, VNL) are trained on the ScanNet dataset. To demonstrate the ability to swap in a predictive camera pose prior, we also evaluate CPP_{pred} using a camera pose predictor trained on a subset of ScanNet excluding any frames from those scenes contained in the test set. The pose

Models	↓ better		↑ better	
	Abs-Rel/Sq-Rel/RMS-log		δ^1 / δ^2	
Trained on NYUv2 (about 120k images)				
VNL	.252	.184	.294	.578 / .876
Trained on InteriorNet Subsets (10k images)				
VNL-N	.241	.172	.323	.549 / .842
Vanilla-N	.283	.209	.330	.485 / .832
CPP-N	.206	.142	.297	.599 / .876
CPP _{pred} -N	.229	.168	.320	.540 / .848
VNL-U	.251	.184	.340	.511 / .829
Vanilla-U	.286	.202	.325	.475 / .833
CPP-U	.200	.139	.288	.612 / .881
CPP _{pred} -U	.235	.176	.321	.540 / .848

Table 3: State-of-the-art comparison among VNL, Vanilla, CPP and CPP_{pred} on the real-world test set sampled from ScanNet. We evaluate the original VNL model that was trained on 120k real-world RGBD images from NYUv2 dataset as well as a VNL model trained from scratch on InteriorNet *Natural* and *Uniform* training set denoted as VNL-N and VNL-U, respectively. The CPP encodes the true camera pose for each ScanNet test image. CPP_{pred} uses a separate camera pose prediction model trained on 10k images from ScanNet (excluding those from the scenes used for testing). Despite being trained on only 10k synthetic images, CPP outperforms VNL by a notable margin. CPP_{pred} performs on-par with VNL having only used inexpensive, low-dimensional pose supervision to train the pose predictor. This suggests pose-conditional prediction is far less data hungry and offers a superior strategy for handling domain shift.

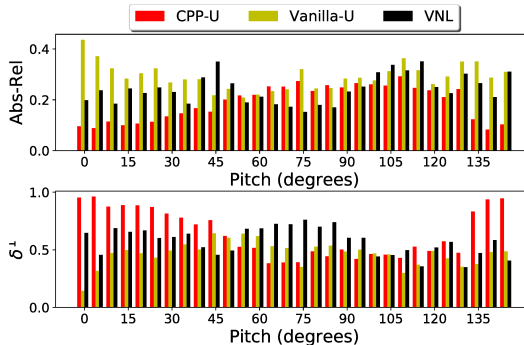


Figure 7: Breakdown of performance w.r.t camera pitch values. We show the bar charts of depth prediction performance as a function of camera pitch, measured by *Abs-Rel* (lower is better) and δ^1 (higher is better), respectively. The vanilla model performs poorly on extreme pitches (e.g., pitch θ close to 0° or 135°). VNL (trained on 120k real images) produces the best predictions but only over a limited range of pitches (roughly between 60° to 90°). The CPP model reduces error over the vanilla model at almost all pitches with the most significant reductions for extreme pitches.

predictor only needs 2-dof camera pose ground-truth which is significantly lower-dimensional and cheaper to acquire than full depth supervision.

We summarize salient results from the quantitative comparisons listed in Table 3.

- On the real test-set, VNL performs better than the vanilla model which likely has to do with synthetic-real domain gap [32] and small training set (10k vs 120k images). However, CPP substantially outperforms VNL! To understand why, we breakdown the performance in Figure 7, from which we clearly see CPP performs remarkably better on images captured at “non-upright” camera pitches, e.g., pitch $\theta < 60^\circ$ or $> 120^\circ$. We visualize two images along with predictions by CPP and VNL in Figure 4 where VNL performs poorly when the camera is posed far from horizontal. This reinforces the claim that separately encoding pose helps the depth predictor generalize much better to novel camera pose distributions and suggests shifts in camera pose statistics may be more important than object shape or low-level appearance in explaining the performance in synthetic-to-real domain adaption.
- We train VNL models on the synthetic InteriorNet train-sets to verify there is nothing special about the distribution of our training data. Our re-implemented VNL models do perform better than vanilla models (refer to the supplementary material). This is natural since VNL is a significantly more sophisticated method than the vanilla model (on both InteriorNet and ScanNet test-sets). However, it does not perform as well as our CPP models when a strong pose prior is available. This largely confirms that our CPP model indeed helps train better depth predictors w.r.t performance and generalization.
- With predicted camera pose, CPP_{pred} outperforms both vanilla and VNL models. This shows that the predicted camera poses serve as useful prior although they could be erroneous (recall our resilience study in Table 5). This further justifies the effectiveness of our factored model which allows for swapping in new test-time camera pose priors.

5 Conclusion

Our experimental analysis confirms that typical learned monocular depth predictors do not generalize well on test scenes which have significantly different camera pose distributions. To address this problem, we propose to train a pose-conditional depth predictor that can exploit camera pose as prior (CPP). We find that exploiting camera poses not only improves depth prediction but also makes the trained predictors generalize much better. When a strong pose prior is not available, training a separate pose predictor still yields many of these benefits despite the lack of “optimal” end-to-end learning. The results hold when evaluating transfer to real-world data where we show that the CPP model, although trained on *synthetic* data, outperforms the state-of-the-art model which is trained on 10x more, *real* data. Our work gives hope that the underlying camera pose problem is more within grasp than one has hoped, suggesting the value of camera poses in learning predictive models.

Acknowledgements This research was supported by NSF grants IIS-1813785, IIS-1618806, a research gift from Qualcomm, and a hardware donation from NVIDIA.

References

- [1] I. Armeni, A. Sax, A. R. Zamir, and S. Savarese. Joint 2D-3D-Semantic Data for Indoor Scene Understanding. *ArXiv e-prints*, February 2017.
- [2] Jiawang Bian, Zhichao Li, Naiyan Wang, Huangying Zhan, Chunhua Shen, Ming-Ming Cheng, and Ian Reid. Unsupervised scale-consistent depth and ego-motion learning from monocular video. In *Advances in Neural Information Processing Systems*, pages 35–45, 2019.
- [3] Angela Dai, Angel X Chang, Manolis Savva, Maciej Halber, Thomas Funkhouser, and Matthias Nießner. Scannet: Richly-annotated 3d reconstructions of indoor scenes. In *Proceedings of the IEEE Conference on Computer Vision and Pattern Recognition*, pages 5828–5839, 2017.
- [4] Tom van Dijk and Guido de Croon. How do neural networks see depth in single images? In *Proceedings of the IEEE International Conference on Computer Vision*, pages 2183–2191, 2019.
- [5] David Eigen and Rob Fergus. Predicting depth, surface normals and semantic labels with a common multi-scale convolutional architecture. In *Proceedings of the IEEE international conference on computer vision*, pages 2650–2658, 2015.
- [6] David Eigen, Christian Puhrsch, and Rob Fergus. Depth map prediction from a single image using a multi-scale deep network. In *Advances in neural information processing systems*, pages 2366–2374, 2014.
- [7] Jose M Facil, Benjamin Ummenhofer, Huizhong Zhou, Luis Montesano, Thomas Brox, and Javier Civera. Cam-convs: camera-aware multi-scale convolutions for single-view depth. In *Proceedings of the IEEE Conference on Computer Vision and Pattern Recognition*, pages 11826–11835, 2019.
- [8] Huan Fu, Mingming Gong, Chaohui Wang, Kayhan Batmanghelich, and Dacheng Tao. Deep ordinal regression network for monocular depth estimation. In *Proceedings of the IEEE Conference on Computer Vision and Pattern Recognition*, pages 2002–2011, 2018.
- [9] Andreas Geiger, Philip Lenz, and Raquel Urtasun. Are we ready for autonomous driving? the kitti vision benchmark suite. In *Proceedings of the IEEE Conference on Computer Vision and Pattern Recognition*, 2012.
- [10] Clément Godard, Oisín Mac Aodha, and Gabriel J Brostow. Unsupervised monocular depth estimation with left-right consistency. In *Proceedings of the IEEE Conference on Computer Vision and Pattern Recognition*, pages 270–279, 2017.
- [11] Xiaoyang Guo, Hongsheng Li, Shuai Yi, Jimmy Ren, and Xiaogang Wang. Learning monocular depth by distilling cross-domain stereo networks. In *Proceedings of the European Conference on Computer Vision (ECCV)*, pages 484–500, 2018.
- [12] Kaiming He, Xiangyu Zhang, Shaoqing Ren, and Jian Sun. Deep residual learning for image recognition. In *Proceedings of the IEEE conference on computer vision and pattern recognition*, pages 770–778, 2016.
- [13] Lei He, Guanghui Wang, and Zhanyi Hu. Learning depth from single images with deep neural network embedding focal length. *IEEE Transactions on Image Processing*, 27(9):4676–4689, 2018.
- [14] Derek Hoiem, Alexei A Efros, and Martial Hebert. Automatic photo pop-up. In *ACM SIGGRAPH 2005 Papers*, pages 577–584. 2005.
- [15] Diederik P Kingma and Jimmy Ba. Adam: A method for stochastic optimization. *arXiv preprint arXiv:1412.6980*, 2014.
- [16] Iro Laina, Christian Rupprecht, Vasileios Belagiannis, Federico Tombari, and Nassir Navab. Deeper depth prediction with fully convolutional residual networks. In *2016 Fourth international conference on 3D vision (3DV)*, pages 239–248. IEEE, 2016.
- [17] Katrin Lasinger, René Ranftl, Konrad Schindler, and Vladlen Koltun. Towards robust monocular depth estimation: Mixing datasets for zero-shot cross-dataset transfer. *arXiv preprint arXiv:1907.01341*, 2019.
- [18] Wenbin Li, Sajad Saeedi, John McCormac, Ronald Clark, Dimos Tzoumanikas, Qing Ye, Yuzhong Huang, Rui Tang, and Stefan Leutenegger. Interiornet: Mega-scale multi-sensor photo-realistic indoor scenes dataset. *arXiv preprint arXiv:1809.00716*, 2018.

- [19] Zhengqi Li, Tali Dekel, Forrester Cole, Richard Tucker, Noah Snavely, Ce Liu, and William T Freeman. Mannequinchallenge: Learning the depths of moving people by watching frozen people. *IEEE Transactions on Pattern Analysis and Machine Intelligence*, 2020.
- [20] Zhengqi Li and Noah Snavely. Megadepth: Learning single-view depth prediction from internet photos. In *Proceedings of the IEEE Conference on Computer Vision and Pattern Recognition*, pages 2041–2050, 2018.
- [21] Fayao Liu, Chunhua Shen, Guosheng Lin, and Ian Reid. Learning depth from single monocular images using deep convolutional neural fields. *IEEE transactions on pattern analysis and machine intelligence*, 38(10):2024–2039, 2015.
- [22] Pushmeet Kohli Nathan Silberman, Derek Hoiem and Rob Fergus. Indoor segmentation and support inference from rgb-d images. In *Proceedings of the European Conference on Computer Vision (ECCV)*, 2012.
- [23] Adam Paszke, Sam Gross, Soumith Chintala, Gregory Chanan, Edward Yang, Zachary DeVito, Zeming Lin, Alban Desmaison, Luca Antiga, and Adam Lerer. Automatic differentiation in pytorch. 2017.
- [24] Ashutosh Saxena, Sung H Chung, and Andrew Y Ng. 3-d depth reconstruction from a single still image. *International journal of computer vision*, 76(1):53–69, 2008.
- [25] Ashutosh Saxena, Min Sun, and Andrew Y Ng. Make3d: Learning 3d scene structure from a single still image. *IEEE transactions on pattern analysis and machine intelligence*, 31(5):824–840, 2008.
- [26] Benjamin Ummenhofer, Huizhong Zhou, Jonas Uhrig, Nikolaus Mayer, Eddy Ilg, Alexey Dosovitskiy, and Thomas Brox. Demon: Depth and motion network for learning monocular stereo. In *Proceedings of the IEEE Conference on Computer Vision and Pattern Recognition*, pages 5038–5047, 2017.
- [27] Yan Wang, Wei-Lun Chao, Divyansh Garg, Bharath Hariharan, Mark Campbell, and Kilian Q Weinberger. Pseudo-lidar from visual depth estimation: Bridging the gap in 3d object detection for autonomous driving. In *Proceedings of the IEEE Conference on Computer Vision and Pattern Recognition*, pages 8445–8453, 2019.
- [28] Wei Yin, Yifan Liu, Chunhua Shen, and Youliang Yan. Enforcing geometric constraints of virtual normal for depth prediction. In *Proceedings of the IEEE International Conference on Computer Vision*, pages 5684–5693, 2019.
- [29] Yurong You, Yan Wang, Wei-Lun Chao, Divyansh Garg, Geoff Pleiss, Bharath Hariharan, Mark Campbell, and Kilian Q Weinberger. Pseudo-lidar++: Accurate depth for 3d object detection in autonomous driving. *arXiv preprint arXiv:1906.06310*, 2019.
- [30] Yinda Zhang, Shuran Song, Ersin Yumer, Manolis Savva, Joon-Young Lee, Hailin Jin, and Thomas Funkhouser. Physically-based rendering for indoor scene understanding using convolutional neural networks. In *Proceedings of the IEEE Conference on Computer Vision and Pattern Recognition*, pages 5287–5295, 2017.
- [31] Shanshan Zhao, Huan Fu, Mingming Gong, and Dacheng Tao. Geometry-aware symmetric domain adaptation for monocular depth estimation. In *Proceedings of the IEEE Conference on Computer Vision and Pattern Recognition*, pages 9788–9798, 2019.
- [32] Yunhan Zhao, Shu Kong, Daeyun Shin, and Charless Fowlkes. Domain decluttering: Simplifying images to mitigate synthetic-real domain shift and improve depth estimation. In *Proceedings of the IEEE Conference on Computer Vision and Pattern Recognition*, 2020.
- [33] Chuanxia Zheng, Tat-Jen Cham, and Jianfei Cai. T2net: Synthetic-to-realistic translation for solving single-image depth estimation tasks. In *Proceedings of the European Conference on Computer Vision (ECCV)*, pages 767–783, 2018.
- [34] Tinghui Zhou, Matthew Brown, Noah Snavely, and David G Lowe. Unsupervised learning of depth and ego-motion from video. In *Proceedings of the IEEE Conference on Computer Vision and Pattern Recognition*, pages 1851–1858, 2017.
- [35] Jun-Yan Zhu, Taesung Park, Phillip Isola, and Alexei A Efros. Unpaired image-to-image translation using cycle-consistent adversarial networks. In *Proceedings of the IEEE international conference on computer vision*, pages 2223–2232, 2017.

Appendices

Outline

In the supplementary material, we provide additional details of training, evaluation and visualization to support our work. We outline this supplement below.

- **Section A: Additional Details in Implementation and Evaluation.** We present further details about our implementation, such as pre-processing the RGB data and training the camera pose prediction models.
- **Section B: Comparisons of Camera Pose Encoding Methods.** We study other methods that encode camera poses in addition to the CPP method as elaborated in the main paper.
- **Section C: Further Study on Real-World Evaluation on ScanNet.** We present in-depth analyses in the real-world evaluation on the ScanNet datasets.
- **Section D: More Visual Results.** We include more depth prediction results of different methods.

A Additional Details in Implementation and Evaluation

A.1 Data Preprocessing

Image and depth preprocessing. All input RGB images are first normalized to the range of $[-1.0, 1.0]$ and then resized to 240×320 before feeding into CNNs. Note that resizing images to 240×320 does not change their original aspect ratios (check detailed intrinsic parameters in Table 6). For better training, as a pre-processing step on the depth [2, 10], we apply the following operation to rescale depth maps y to get a normalized map y' :

$$y' = \left(\frac{y - E_{min}}{E_{max} - E_{min}} - 0.5 \right) * 2.0, \tag{8}$$

where $E_{min} = 1.0$ and $E_{max} = 10.0$ are minimum and maximum evaluation value, respectively. The above operation is a map from $[1.0, 10.0]$ to $[-1.0, 1.0]$. In literature, it is reported the model can be trained better in this scale range [33, 31]. We only compute the loss for pixels that have depth values between 1.0 and 10.0 meters. We evaluate the depth prediction on the original depth scale. To do so, we apply an inverse operation of Eq. 8 to the predicted depth maps. Moreover, we also only evaluate the depth that lies in $[1, 10]$ meters.

A.2 Pose Prediction Network

Training pose predictors. When camera poses are not available during testing, we train a camera pose predictor that predicts camera pitch θ and height h encoded by our CPP_{pred} model. We build the pose predictor over ResNet18 structure with a new top layer that outputs a 2D vector for an input image. To train it, we fine-tune a ResNet18 checkpoint that is pre-trained on ImageNet dataset. We simply use the L1 loss.

A.3 Evaluation Protocol

Evaluation range. We plot the depth statistics of InteriorNet shown in Figure 8. By the histogram, we set the depth range of interest to be $[1.0, 1.0]$ in meters.

Evaluation checkpoint selection. During training, we cache the model checkpoints every 10 epochs. After training, we select the best model with the minimum average L1 loss on the validation set. We report the performance of this selected model.

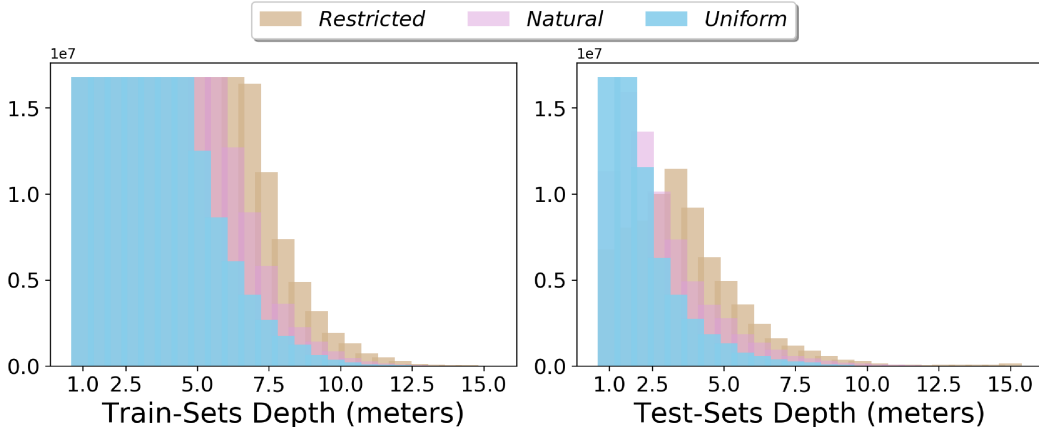


Figure 8: **Frequencies of depth values in the three InteriorNets sets.** We set the depth range as $[1.0, 10.0]$ in this work. Accordingly, we do not train or test on the depth values outside this range.

Models	Natural test-set (N)		Uniform test-set (U)		Restricted test-set (R)	
	↓ lower is better Abs-Rel/Sq-Rel/RMS/RMS-log	↑ better $\delta^1 / \delta^2 / \delta^3$	↓ lower is better Abs-Rel/Sq-Rel/RMS/RMS-log	↑ better $\delta^1 / \delta^2 / \delta^3$	↓ lower is better Abs-Rel/Sq-Rel/RMS/RMS-log	↑ better $\delta^1 / \delta^2 / \delta^3$
Vanilla model – no camera pose encoding						
Vanilla-N	0.154 / 0.148 / 0.694 / 0.229	0.803 / 0.945 / 0.979	0.183 / 0.146 / 0.600 / 0.250	0.724 / 0.926 / 0.978	0.155 / 0.233 / 0.982 / 0.284	0.804 / 0.916 / 0.952
Vanilla-U	0.169 / 0.173 / 0.769 / 0.250	0.767 / 0.935 / 0.975	0.161 / 0.117 / 0.569 / 0.227	0.758 / 0.950 / 0.985	0.178 / 0.283 / 1.084 / 0.325	0.764 / 0.898 / 0.938
Vanilla-R	0.259 / 0.349 / 1.104 / 0.392	0.551 / 0.786 / 0.905	0.284 / 0.307 / 0.898 / 0.376	0.506 / 0.779 / 0.920	0.147 / 0.230 / 0.960 / 0.286	0.820 / 0.918 / 0.952
Encoding model – naive encoding						
Naive-N	0.132 / 0.145 / 0.698 / 0.219	0.835 / 0.944 / 0.978	0.137 / 0.116 / 0.556 / 0.213	0.810 / 0.944 / 0.983	0.165 / 0.231 / 0.979 / 0.276	0.778 / 0.918 / 0.960
Naive-U	0.160 / 0.186 / 0.819 / 0.250	0.774 / 0.924 / 0.971	0.130 / 0.112 / 0.575 / 0.207	0.823 / 0.952 / 0.984	0.192 / 0.290 / 1.130 / 0.316	0.718 / 0.886 / 0.945
Naive-R	0.265 / 0.375 / 1.182 / 0.437	0.519 / 0.744 / 0.870	0.274 / 0.299 / 0.949 / 0.411	0.468 / 0.742 / 0.898	0.146 / 0.237 / 0.983 / 0.293	0.821 / 0.917 / 0.949
Encoding model – camera pose prior (CPP)						
CPP-N	0.108 / 0.120 / 0.629 / 0.199	0.872 / 0.958 / 0.982	0.106 / 0.088 / 0.477 / 0.183	0.876 / 0.961 / 0.985	0.155 / 0.244 / 0.964 / 0.285	0.806 / 0.918 / 0.953
CPP-U	0.129 / 0.150 / 0.693 / 0.221	0.842 / 0.945 / 0.977	0.102 / 0.087 / 0.475 / 0.177	0.889 / 0.966 / 0.987	0.178 / 0.303 / 1.082 / 0.322	0.773 / 0.901 / 0.940
CPP-R	0.223 / 0.263 / 0.884 / 0.308	0.651 / 0.879 / 0.856	0.249 / 0.275 / 0.751 / 0.312	0.620 / 0.873 / 0.953	0.142 / 0.213 / 0.941 / 0.274	0.828 / 0.919 / 0.952
Encoding model – predicted camera pose prior (CPP _{pred})						
CPP _{pred} -N	0.146 / 0.134 / 0.669 / 0.218	0.820 / 0.954 / 0.982	0.166 / 0.121 / 0.565 / 0.231	0.762 / 0.944 / 0.984	0.156 / 0.234 / 0.991 / 0.286	0.803 / 0.918 / 0.954
CPP _{pred} -U	0.168 / 0.187 / 0.790 / 0.252	0.779 / 0.934 / 0.974	0.148 / 0.115 / 0.564 / 0.213	0.806 / 0.953 / 0.984	0.196 / 0.338 / 1.144 / 0.333	0.747 / 0.891 / 0.938
CPP _{pred} -R	0.266 / 0.350 / 1.083 / 0.389	0.554 / 0.789 / 0.906	0.308 / 0.347 / 0.926 / 0.394	0.486 / 0.754 / 0.908	0.143 / 0.214 / 0.945 / 0.276	0.827 / 0.918 / 0.952

Table 4: Detailed comparisons of depth predictions and generalization of naive models against vanilla, CPP, and CPP_{pred} models with all evaluation metrics. Naive-N/U/R are depth predictors trained with naive encoding on *Natural/Uniform/Restricted* train-sets. We find that the performance of naive encoding models are between vanilla and CPP models, indicating encoding camera poses naively still help training a better depth predictor but it is not as effective as CPP encoding.

B Comparison of Camera Pose Encoding Methods

B.1 Encoding Models: Naive Encoding vs CPP Encoding.

Naive encoding converts camera pitch θ and height h into two individual maps that share the same spatial resolution as RGB images. The two maps are then concatenated to RGB images before fed into depth predictors. We compare the naive models in Table 4. In the table, by comparing the performance of models when trained and tested on the same domain (i.e., camera pose distribution), the naive encoding model performs better than the Vanilla model, although it falls short to our CPP model. This largely confirms the benefit of exploiting the camera pose information for depth prediction. Additionally, our CPP model outperforms naive encoding on all three evaluation sets, which demonstrates the effectiveness of our proposed CPP encoding method.

B.2 CPP encoding: Clipping vs. Inverse Tangent Transform

At the last step in computing CPP encoded maps \mathbf{M}_{CPP} , we apply the inverse tangent function to eliminate the infinity values and maps the values of \mathbf{M} (i.e. $\mathbf{M}_{CPP} = \tan^{-1}(\mathbf{M})$) to a reasonable value range, otherwise, \mathbf{M} may have infinite values caused by the vanishing point. In this subsection, we study another straightforward method to transform \mathbf{M} , i.e., clipping \mathbf{M} with a defined threshold.

To clip \mathbf{M} , we set a threshold τ that represents our belief of the distance from camera to the furthest point in the scene. Mathematically, the clipping method results in an encoded map $\mathbf{M}_{CPP-Clip} \in \mathbb{R}^{H \times W}$ as:

$$\mathbf{M}_{CPP-Clip}[u, v] = \begin{cases} M[u, v] & M[u, v] < \tau \\ \tau & \text{otherwise} \end{cases} \quad \forall u \in [0, H], v \in [0, W]$$

Models	↓ better	↑ better
	Abs-Rel/Sq-Rel/RMS/RMS-log	$\delta^1 / \delta^2 / \delta^3$
Trained & Evaluated on InteriorNet <i>Natural</i> Subset		
Naive-N	0.132 / 0.145 / 0.698 / 0.219	0.835 / 0.944 / 0.978
CPP-Clip-N	0.109 / 0.124 / 0.639 / 0.204	0.873 / 0.956 / 0.981
CPP-N	0.108 / 0.120 / 0.629 / 0.199	0.872 / 0.958 / 0.982
Trained & Evaluated on InteriorNet <i>Uniform</i> Subset		
Naive-U	0.130 / 0.112 / 0.575 / 0.207	0.823 / 0.952 / 0.984
CPP-Clip-U	0.111 / 0.103 / 0.516 / 0.193	0.869 / 0.957 / 0.984
CPP-U	0.102 / 0.087 / 0.475 / 0.177	0.889 / 0.966 / 0.987
Trained & Evaluated on InteriorNet <i>Restricted</i> Subset		
Naive-R	0.146 / 0.237 / 0.983 / 0.293	0.821 / 0.917 / 0.949
CPP-Clip-R	0.147 / 0.246 / 0.998 / 0.297	0.821 / 0.915 / 0.946
CPP-R	0.142 / 0.213 / 0.941 / 0.274	0.828 / 0.919 / 0.952

Table 5: Comparisons of different encoding methods evaluated on InteriorNet test-sets. Naive encoding converts camera pitch and height into two separate channels. CPP applies an inverse tangent transform (\tan^{-1}) in encoding the camera poses. In contrast, CPP-Clip replaces the \tan^{-1} function with a clipping operation while keeping every other step same as CPP encoding. From the quantitative results, CPP encoding outperforms the other two. This shows the effectiveness of our CPP encoding method along with the \tan^{-1} operation.

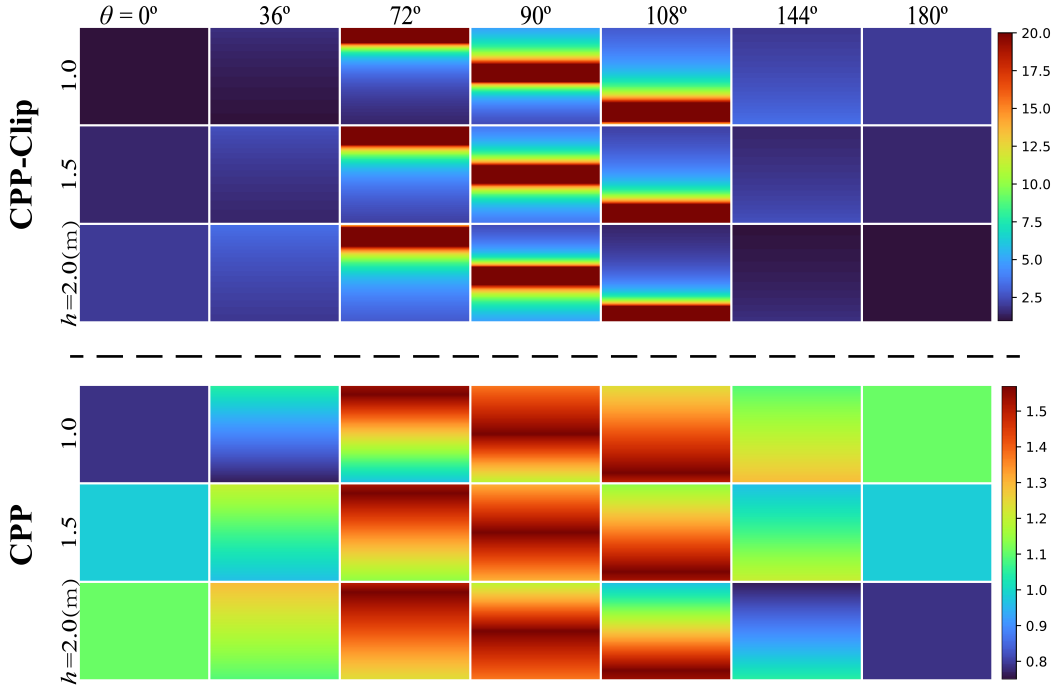


Figure 9: Visual comparisons of encoded maps of CPP and CPP-Clip. We set the threshold $\tau = 20.0$ for CPP-Clip. Encoding maps by CPP-Clip capture horizon with the “red stripe”.

We set $\tau = 20.0$ in this work. After clipping, we also rescale the encoded map to the range of $[-1.0, 1.0]$ to match the statistics of RGB images. We find this yields better performance than directly concatenate $M_{CPP-Clip}$ with RGB images. We visually compare some encoded maps in Figure 9, where we see the clipping method introduces “artifacts” (non-smoothing stripes not desired in training). As shown in Table 5, CPP-Clip does not perform as well as CPP that adopts inverse tangent transform. Additionally, we note that CPP-Clip has a worse performance when trained and tested on the *Restricted* set. This implies the “artificial stripe” introduced by clipping³ is indeed undesirable for training depth predictors.

³All the clipped encoding maps contain a stripe because the vanishing point is always visible in the camera pitch ($\sim 90^\circ$).

	InteriorNet	NYUv2	ScanNet
Original RGB Images			
Focal Length	$f_x = f_y = 600$	$f_x \sim f_y \sim 581$	$f_x \sim f_y \sim 1168$
Resolution	480×640	480×640	968×1296
Field of View (fov)	$fov_x = 43.60^\circ$ $fov_y = 56.14^\circ$	$fov_x = 44.89^\circ$ $fov_y = 57.69^\circ$	$fov_x = 45.02^\circ$ $fov_y = 58.04^\circ$
Resized RGB Images			
Focal Length	$f_x = f_y = 300$	$f_x \sim f_y \sim 290$	$f_x \sim f_y \sim 288$
Resolution	240×320		
Field of View (fov)	$fov_x = 43.60^\circ$ $fov_y = 56.14^\circ$	$fov_x = 44.96^\circ$ $fov_y = 57.77^\circ$	$fov_x = 45.24^\circ$ $fov_y = 58.11^\circ$

Table 6: The detailed statistics of intrinsic parameters of InteriorNet, NYUv2, and ScanNet. After resizing, the intrinsic parameters of all three datasets are very close. This filter out the factors that may be caused by camera models when we study the generalizability of depth predictors.

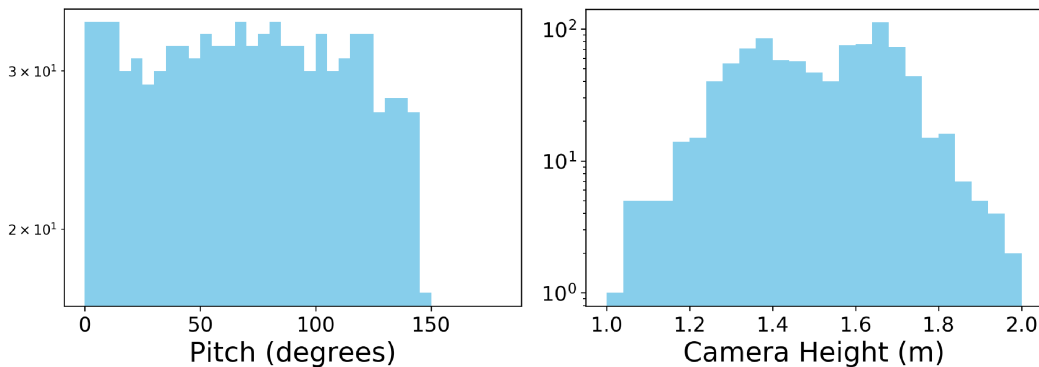


Figure 10: Histogram of the pitch and camera height of ScanNet sampled test-set. This test-set is built by sampling images by having their pitch angles approaching a uniform distribution. We evaluate VNL, vanilla, CPP, CPP_{pred} trained on InteriorNet *Natural* and *Uniform* train-sets, and VNL trained on the real-world dataset, NYUv2 (about 120k) on this test-set. The quantitative results with all evaluation metrics are shown in Table 7.

C Further Study on Real-World Evaluation on ScanNet

In the main paper, we have experiments where models are trained and evaluated on different datasets (e.g., training on InteriorNet/NYUv2 while testing on ScanNet). The purpose of this experiment is not only to evaluate the effectiveness of CPP on a real-world dataset but also to compare CPP against state-of-the-art depth predictors.

C.1 Intrinsic Parameters of InteriorNet, NYUv2, and ScanNet

We list the detailed intrinsic parameters of all three datasets in Table 6. The intrinsic parameters of RGB images (after resizing) from the three datasets are close to each other. This demonstrates that the three datasets are “close” enough w.r.t camera model, implying that we can study how trained depth predictors can generalize to different domains while keeping the camera model similar.

C.2 Camera Pose Distribution of ScanNet Evaluation Set

In the main paper, we build a ScanNet test-set to validate the performance of CPP and compare it against other models, including the state-of-the-art model, VNL. This test-set shares the same high-level idea as the InteriorNet *Uniform* set as the camera pose distribution approaches the uniform distribution. We plot the camera pose distribution of the evaluation set sampled from ScanNet in Figure 10 to provide an intuitive illustration and a clear comparison against InteriorNet sampled sets.

C.3 Training VNL on InteriorNet Train-Sets

In the main paper, we evaluate VNL that is trained on NYUv2 dataset (about 120k image/depth pairs). To provide a thorough comparison, we train VNL on InteriorNet *Natural* and *Uniform* train-sets denoted as VNL-N and VNL-U, respectively. The quantitative results of VNL-N / U and other

Models	↓ better	↑ better
	Abs-Rel/Sq-Rel/RMS/RMS-log	$\delta^1 / \delta^2 / \delta^3$
Trained on NYUv2 (about 120k images)		
VNL	0.252 / 0.184 / 0.576 / 0.294	0.578 / 0.876 / 0.971
Trained on InteriorNet Subsets (10k images)		
VNL-N	0.241 / 0.172 / 0.624 / 0.323	0.549 / 0.842 / 0.956
Vanilla-N	0.283 / 0.209 / 0.640 / 0.330	0.485 / 0.832 / 0.960
CPP-N	0.206 / 0.142 / 0.608 / 0.297	0.599 / 0.876 / 0.968
CPP _{pred} -N	0.229 / 0.168 / 0.646 / 0.320	0.540 / 0.848 / 0.960
VNL-U	0.251 / 0.184 / 0.655 / 0.340	0.511 / 0.829 / 0.948
Vanilla-U	0.286 / 0.202 / 0.627 / 0.325	0.475 / 0.833 / 0.972
CPP-U	0.200 / 0.139 / 0.594 / 0.288	0.612 / 0.881 / 0.969
CPP _{pred} -U	0.235 / 0.176 / 0.645 / 0.321	0.540 / 0.848 / 0.959

Table 7: Quantitative results of Vanilla, CPP, CPP_{pred}, and VNL evaluated on ScanNet test-set. In this table, we report seven metrics widely used in literature.

Models	↓ better	↑ better
	Abs-Rel/Sq-Rel/RMS/RMS-log	$\delta^1 / \delta^2 / \delta^3$
Trained & Evaluated on InteriorNet <i>Natural</i> Subset		
VNL-N	0.131 / 0.132 / 0.697 / 0.220	0.845 / 0.953 / 0.980
Vanilla-N	0.154 / 0.148 / 0.694 / 0.229	0.803 / 0.945 / 0.979
CPP-N	0.108 / 0.120 / 0.629 / 0.199	0.872 / 0.958 / 0.982
CPP _{pred} -N	0.146 / 0.134 / 0.669 / 0.218	0.820 / 0.954 / 0.982
Trained & Evaluated on InteriorNet <i>Uniform</i> Subset		
VNL-U	0.148 / 0.106 / 0.574 / 0.220	0.796 / 0.955 / 0.985
Vanilla-U	0.161 / 0.117 / 0.569 / 0.227	0.758 / 0.950 / 0.985
CPP-U	0.102 / 0.087 / 0.475 / 0.177	0.889 / 0.966 / 0.987
CPP _{pred} -U	0.148 / 0.115 / 0.564 / 0.213	0.806 / 0.953 / 0.984

Table 8: Quantitative results of VNL trained and evaluated on InteriorNet test-sets. We train VNL ourselves on InteriorNet *Natural* and *Uniform* train-sets. We find that VNL has a clear advantage over vanilla models, demonstrating the effectiveness of its sophisticated loss design.

comparable models are shown in Table 8. Without any surprises, VNL is better than vanilla models due to the significantly more sophisticated loss design. Together with all other observations in the main paper, we believe it is conclusive that CPP models indeed help train better depth predictors w.r.t. performance and generalization.

C.4 NYUv2 Raw Data Tilt Angle Distribution

In the main paper, we breakdown the depth prediction of Vanilla, VNL (trained on NYUv2), and CPP by pitch angle to illustrate the effectiveness of CPP on various pitch angles. We observe that VNL outperforms CPP models when pitch angles are in the range approximately from 60° to 90°. We conjecture this is because the camera pitch angles of NYUv2 images are also in this range. To verify this explanation, we plot the histogram of the tilt angles of NYUv2 raw dataset in Figure 11. Note that tilt angles are close to pitch angles in NYUv2 dataset since the roll angles are almost negligibly small.

Concretely, we download the NYUv2 raw dataset from their official website⁴. Synchronize the RGB, depth, and accelerometer data with the provided function in the official toolbox and then plot the histogram with the decoded accelerometer data. It is easy to observe that the tilt angles in the NYUv2 are densely distributed roughly from 50° to 100°, which explains why VNL is particularly strong between 60° to 90°.

D More Visual Results

We provide more depth prediction results of vanilla, naive, CPP, and VNL (trained on NYUv2) models on InteriorNet and ScanNet showing in Figure 12 and Figure 13, respectively.

Success cases/Visual improvements. We observe that CPP performs surprisingly well on images shown in the first and the last rows in Figure 12. For other images in Figure 12, CPP also performs

⁴NYUv2 website: https://cs.nyu.edu/~silberman/datasets/nyu_depth_v2.html

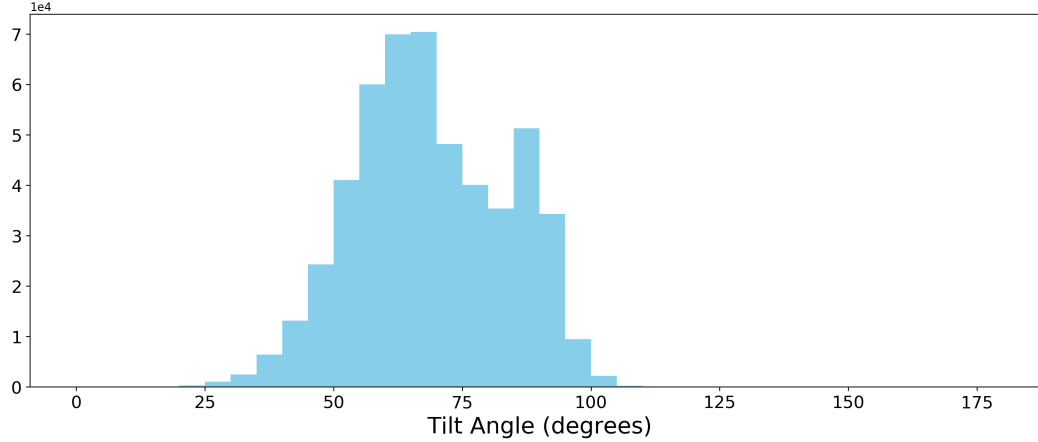


Figure 11: Histogram of tilt angles in NYUv2 raw dataset. In NYUv2 dataset, the tilt angle is close enough to pitch since roll angles are almost negligibly small. It is easy to observe that the tilt angles are mostly in the range between 50° to 100° . By training with a large amount of NYUv2 RGBD data, VNL performs particularly well in pitch angles between 60° and 90° , and better than CPP in this range when tested on ScanNet test-set. However, CPP outperforms VNL at the other pitch angles, this demonstrates the benefit of exploiting camera poses for depth prediction.

clearly better than vanilla models. This shows the advantages of encoding camera poses for depth prediction. When evaluated on ScanNet test-set (shown in Figure 13), CPP models significantly outperform Vanilla and VNL in terms of predicted depth scales. In contrast, other methods introduce obvious scale ambiguities in their predictions.

Failure cases/Potential improvements. Admittedly, CPP models are not perfect and there are many potential improvements just based on visual inspections. CPP shows similar performance as Vanilla model when pitch angles are around 90° and scene content becomes complicated (check examples in row-4 and 5 in Figure 12). Moreover, VNL is able to capture local structures, such as object boundaries than CPP models. But CPP makes overly smooth predictions. We conjecture the reason is that VNL is trained on 10X more RGBD data than our CPP model.

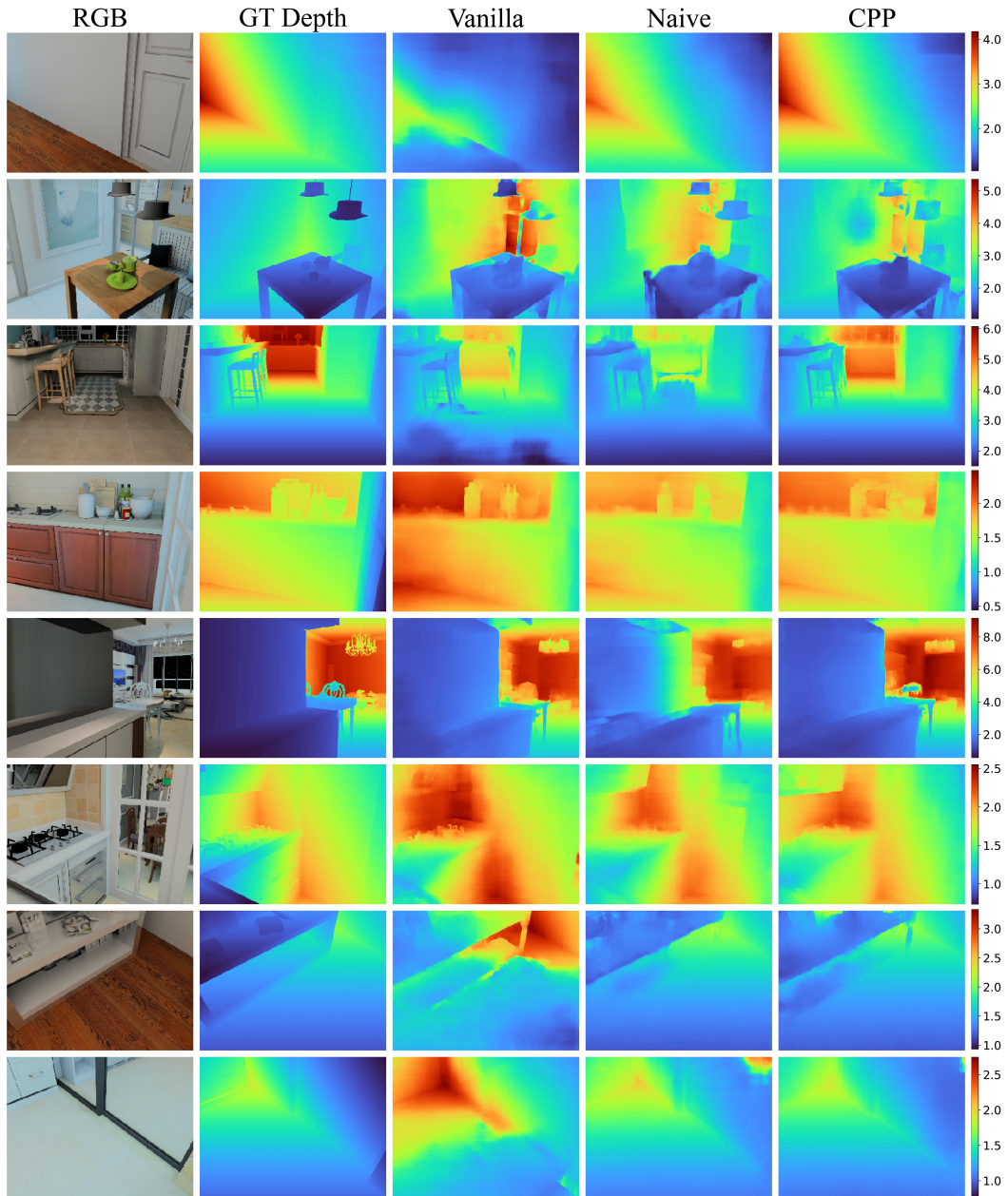


Figure 12: Depth predictions of Vanilla, naive, and CPP models on InteriorNet dataset. Naive models are depth predictors trained with the naive encoding described in Section B.1.

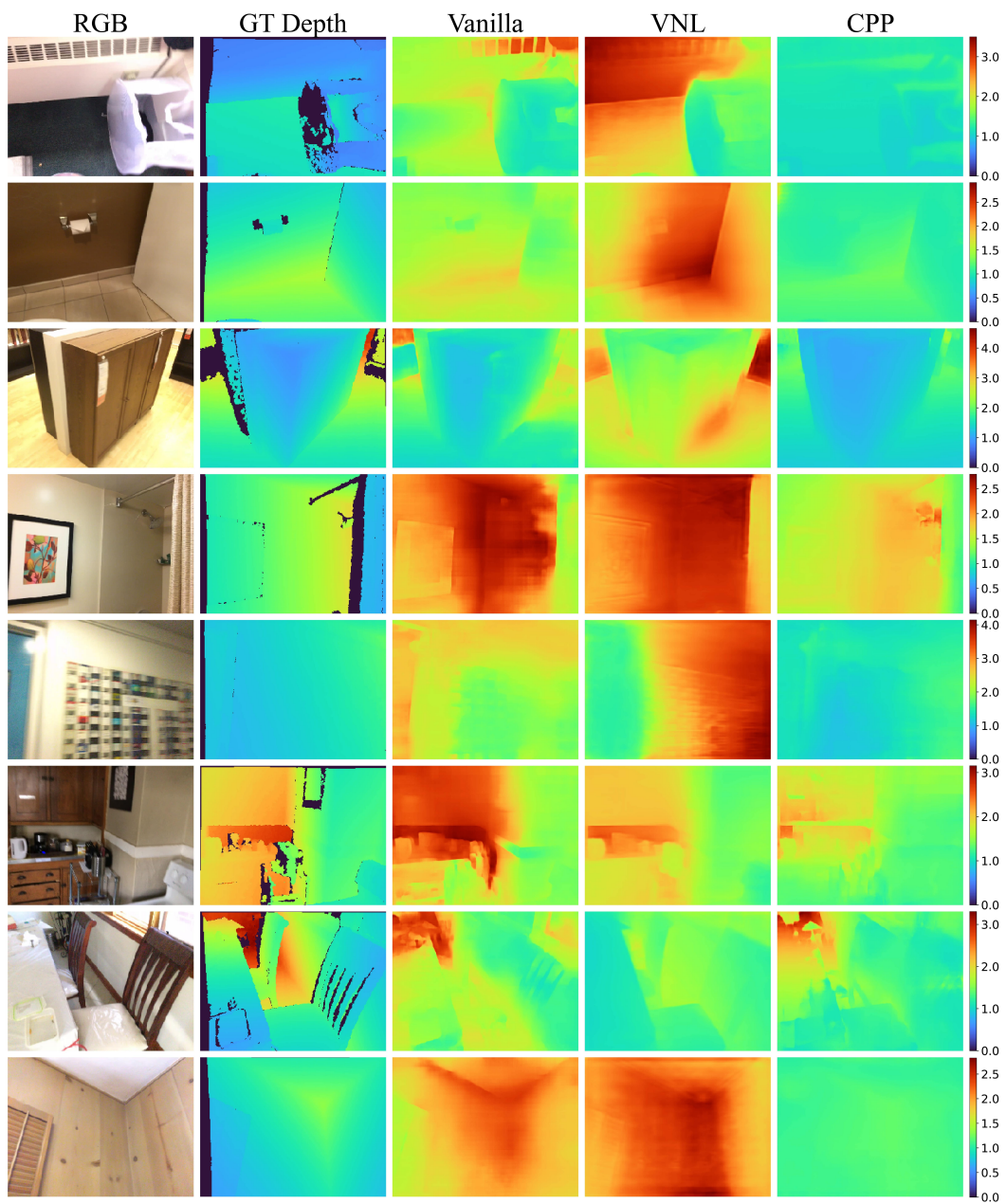


Figure 13: Depth predictions of Vanilla, VNL (trained on NYUv2), and CPP models on ScanNet dataset.